Dependence of Raman spectra G' band intensity on metallicity of single-wall carbon nanotubes

Ki Kang Kim,[1] Jin Sung Park,[2] Sung Jin Kim,[1] Hong Zhang Geng,[1] Kay Hyeok An,[3] Cheol-Min Yang,[1]
Kentaro Sato,[2] Riichiro Saito,[2,*,†] and Young Hee Lee[1,*,‡]

[1]*Department of Physics, Center for Nanotubes and Nanostructured Composites, Institute of Basic Sciences, Sungkyunkwan University,
Suwon 440-746, Republic of Korea*
[2]*Department of Physics, Tohoku University and CREST, Sendai 980-8578, Japan*
[3]*Material & Development Department, Jeonju Machinery Research Center, Jeonju 561-844, Republic of Korea*

We report the peculiar behavior of the G' band Raman intensity, which is dependent on the metallicity of single-wall carbon nanotubes (SWCNTs). In the metallic SWCNTs, the G' band intensity was enhanced relative to the G band intensity, while the G' band intensity was suppressed in the semiconducting SWCNTs. Resonance Raman spectroscopy (using laser energies of $E_{laser}=2.41$, 1.96, 1.58, and 1.165 eV) showed these features on the metal-enriched and semiconducting-enriched SWCNT samples that had been selectively separated by the nitronium ions. The metallicity dependence was explained theoretically by calculating the resonance Raman intensity within the extended tight-binding calculations. The calculated results confirm that the G' band intensity of the metallic SWCNTs is stronger than that for the semiconducting SWCNTs because the electron-phonon matrix elements for the TO phonon at the K point is larger for metallic SWCNTs and the resonance window for E_{33}^{S} is larger than that for E_{11}^{M}.

I. INTRODUCTION

Carbon nanotubes show peculiar electronic structures due to their one-dimensional geometry with a diameter on the nanometer scale. The momentum of the electrons is quantized along the circumferential direction, and the electronic structures of carbon nanotubes depend strongly on the geometrical structure represented by the chiral index (n,m). In general, when $n-m=3p$, where p is an integer, carbon nanotubes become metallic, and semiconducting when $n-m \neq 3p$.[1,2] This is valid for nanotubes with diameters greater than 1.0 nm, in which curvature induced narrow band gap for metallic nanotubes can be neglected in Raman spectroscopy.[3] The electronic structures of single-wall carbon nanotubes (SWCNTs) have been studied extensively by resonance Raman spectroscopy,[4] optical absorption spectroscopy,[5] and photoluminescence[6] (or fluorescence[7]) spectroscopy.

The presence of van Hove singularities (vHs) in the electronic structures of SWCNTs has opened a new research area in resonance Raman spectroscopy of solids.[8] The discrete position of the vHs in the electronic joint density of states (E_{ii}) depends strongly on the chirality and diameter of the SWCNTs. Resonance Raman spectroscopy can be used to assign (n,m) values from a plot of E_{ii} as a function of the diameter of the SWCNT (the Kataura plot).[9,10] SWCNTs are synthesized by arc discharge,[11] laser ablation,[12] and chemical vapor deposition.[13] These processes result in the production of SWCNTs with various chiral indices and metallicities. Therefore, an assignment of (n,m) and metallicity by Raman spectroscopy is essential for evaluating these materials.

The chirality of SWCNTs can be identified using the radial breathing mode (RBM) in Raman spectroscopy.[10] The RBMs are inversely proportional to the diameter of the SWCNTs, $\omega(\text{cm}^{-1})=a/d_t(\text{nm})+b$, where d_t is the diameter of the SWCNT, and a and b are constants that vary according to

the environment such as the bundle or substrate. For example, $a=248$ and $b=0$ for isolated nanotubes on a SiO_2 substrate, and $a=234$ and $b=10$ for bundles.[10,14] However, the assignment becomes difficult for a relatively higher E_{ii} and a larger d_t because there are many overlaps of (n,m) in the Kataura plot between semiconducting and metallic SWCNTs. G band spectra might be able to distinguish between metallic and semiconducting SWCNTs in the Raman spectra, where the separation of frequencies for the split G band ($G+$ and $G-$) has a different diameter dependence and a different spectral shape.[15] This discussion is difficult because the G band Raman intensity strongly depends on the chiral angle,[15] particularly for a SWCNT with a chiral angle near a zigzag nanotube.[16] Therefore, simple information on the metallicity of SWCNT by Raman spectroscopy is desired.

In this paper, we demonstrate that the G' band (Raman signal[4] near 2600 cm^{-1}) intensity shows a strong dependence on the metallicity of the sample. The G' band usually has a higher intensity in SWCNTs than the D band because the G' band is caused by two-phonon scattering processes that are free from the defect structures, while the D band consists of elastic and inelastic scattering processes.[17] The metallicity dependence of the G' band intensity relative to the G band intensity was observed by separating the metal-enriched or semiconducting-enriched SWCNT samples by the oxidation of nitronium ions.

The experimental results were confirmed by calculating the resonance Raman intensity for the G' band using the double resonance Raman scattering theory.[17] Since the G' band corresponds to a two-phonon scattering process of phonons around the K point (hexagonal corners of two-dimensional Brillouin zone), the Raman intensity can be calculated as a function of the laser excitation energy E_{laser} using the electron-photon[18] and electron-phonon matrix elements for each (n,m) value.[19] Recently, there was a report on the exciton effect for the Raman intensity.[20] However, this
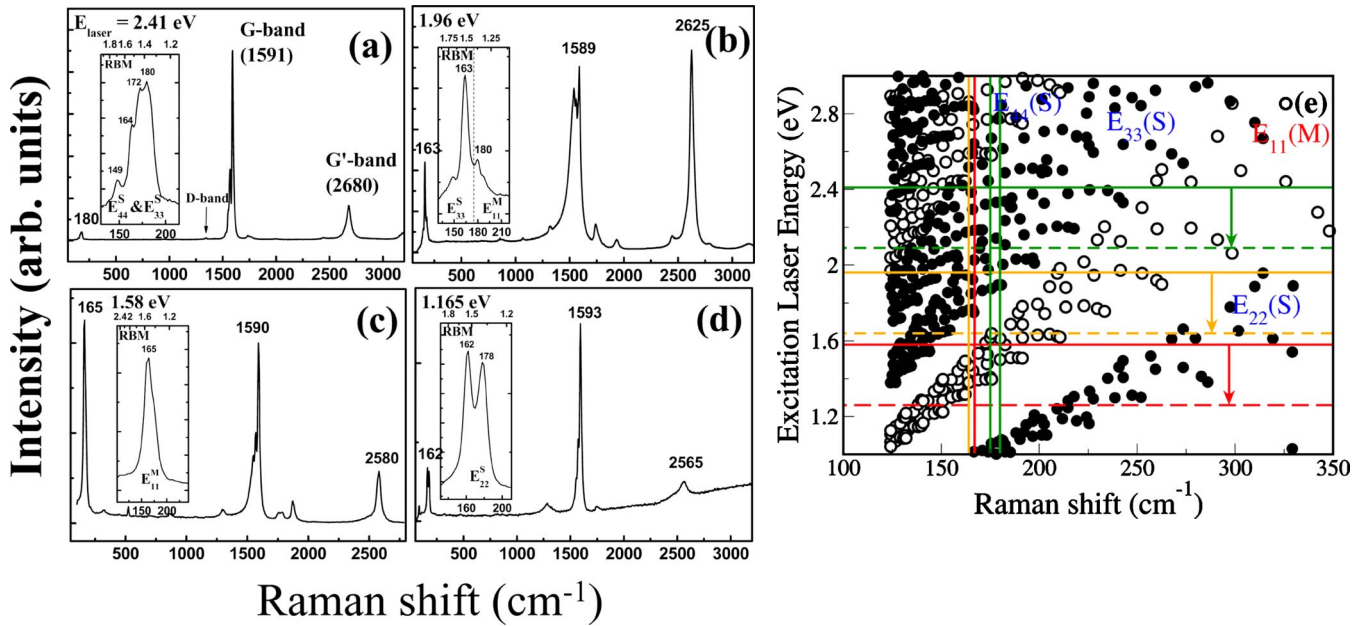
FIG. 1. (Color online) Raman spectra at various excitation energies of the SWCNT sample: (a) 2.41 eV, (b) 1.96 eV, (c) 1.58 eV, and (d) 1.165 eV. All Raman spectra were normalized to the G band intensity. The inset in each figure is the enlarged radial breathing mode. The numbers in each figure are the diameters of the corresponding peaks in nm (upper axis) and phonon frequencies (bottom axis). $E_{ii}^{S(M)}$ indicate the van Hove singularity transition energy between the ith levels of the semiconducting (metallic) SWCNT. (e) Kataura plot obtained from extended tight-binding model. The solid and dashed lines are incident laser energies and the corresponding scattered energies used in our experiment. The arrows indicate the scattered photons of the corresponding peaks of (a)–(c). The green, yellow, and red vertical lines are positions of main RBM peak in (a), (b), and (c), respectively.

study did not use the exciton-phonon and exciton-photon interactions but instead used the electron-phonon and electron-photon interactions for simplicity. This is because the exciton-phonon interaction gives a similar value to the electron-phonon interaction, and the exciton-photon interaction does not change the relative intensity.[20] It was shown that the present calculation could explain the metallicity dependence. The G' band intensity calculation by the exciton wave functions will be reported elsewhere.

In Sec. II, we will explain the experimental method and details of the calculation. In Sec. III, experimental results for Raman spectra for several laser energies and theoretical results are presented. We will compare the experimental results with the calculated results. In Sec. IV, the discussion and summary are given.

II. METHOD

The dependence of the G' band intensity on the metallicity of SWCNTs has been observed by resonance Raman spectroscopy (Renishaw, microprobe RM1000-Invia). Several excitation energies of 2.41 eV (514 nm, Ar$^+$ ion laser), 1.96 eV (632.8 nm, He-Ne laser) with a notch filter, which accepts a spectral range of $50-4000$ cm^{-1}, and 1.58 eV (785 nm, diode laser) with a notch filter ($100-3600$ cm^{-1}) were used in this study. Fourier transformed Raman (Bruker IFS-66/S) spectroscopy was also carried out with an excitation energy of 1.165 eV [1064 nm, Nd:YAG (YAG denotes yttrium aluminum garnet) laser] using the Rayleigh line rejection filter with a spectral range of $70-3600$ cm^{-1}.

Two types of pristine SWCNT samples were used in these measurements. One type was highly purified SWCNTs synthesized by arc discharge (Iljin Nanotech), with diameters ranging from 1.4 to 1.6 nm.[21] Another type is the high pressure carbon monoxide (HiPCO) SWCNTs (Carbon Nanotechnologies Inc.) with diameters ranging from 0.8 to 1.3 nm. The HiPCO sample was further treated by nitronium ions to remove the metallic SWCNTs.[22,23] In this treatment, 10 mg of the pristine sample were sonicated for 24 h in tetramethylene sulfone/chloroform (1:1 by weight) containing 50 mmol nitronium hexafluoroantimonate (NHFA). Details of the sample preparation have been reported elsewhere.[22] A previous paper discussed the sample qualities determined by RBM and G band Raman spectroscopy.[23] The semiconducting SWCNTs were chosen particularly for their small diameters (<1 nm). The acid-treated samples (HNO$_3$:H$_2$SO$_4$=1:9 by volume ratio) were also used in this experiment.[23]

The experimental results were compared by calculating the two-phonon scattering processes for the G' band intensity using the extended tight-binding (ETB) method.[19] The electronic energy dispersion of a SWCNT was obtained using the ETB method, in which $2p_z$, $2p_y$, $2p_x$, and $2s$ atomic orbitals are taken into account to reproduce the E_{ii} values for a SWCNT, particularly for a smaller diameter SWCNT. The phonon dispersion relation, $\hbar\omega$, was calculated using a force-constant tight-binding model, in which the force constant was taken up to the 20th nearest neighbor atomic sites given by Dubay and Kresse,[24] which reproduce the phonon dispersion obtained by inelastic x-ray scattering. The Raman inten-
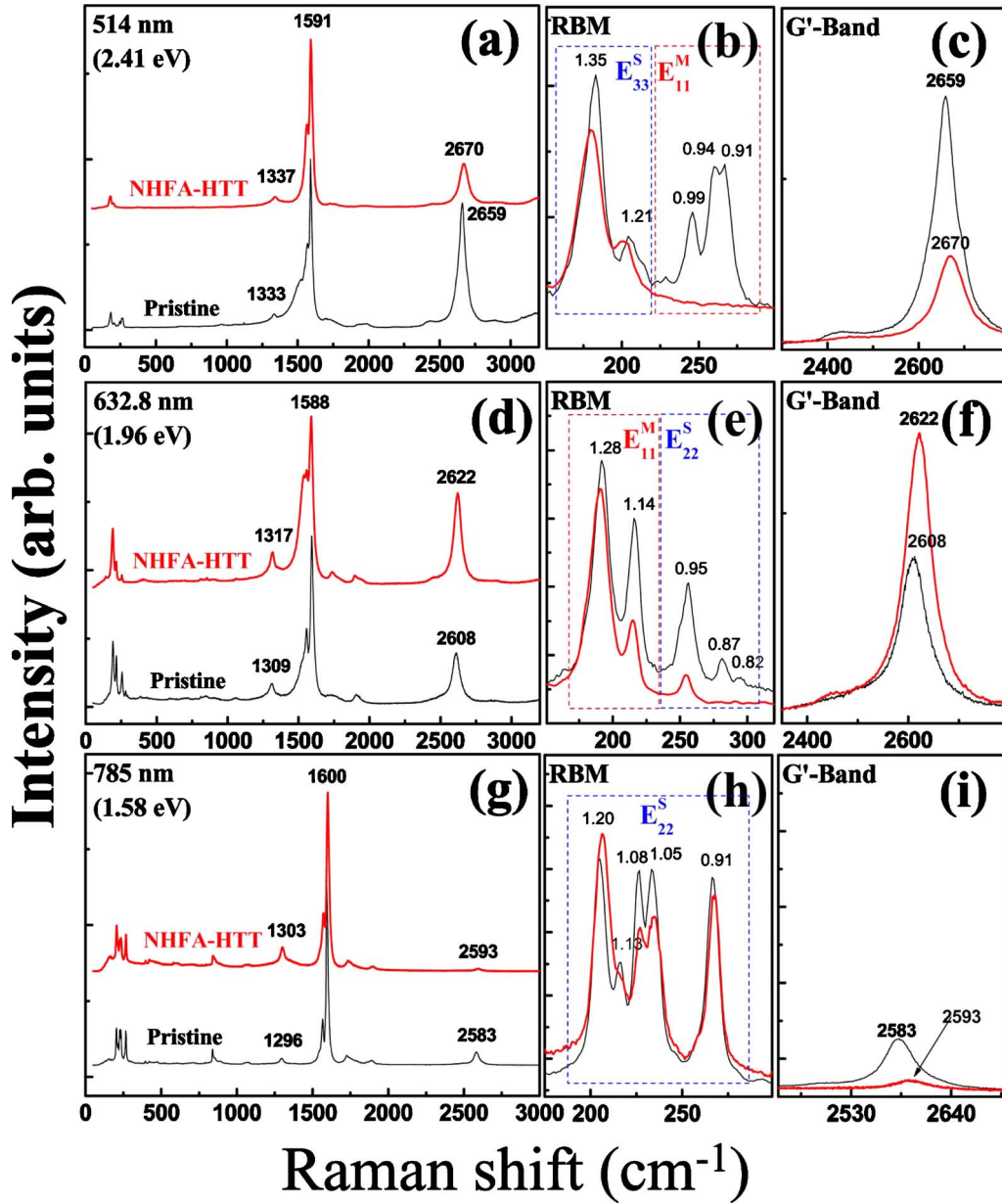
FIG. 2. (Color online) Raman spectra of (bottom) the pristine HiPCO sample and (top) the NHFA-treated HiPCO sample at excitation energies of [(a)–(c)] 2.41 eV, [(d)–(f)] 1.96 eV, and [(g)–(i)] 1.58 eV. The notations are the same as shown in Fig. 1.

sity for the G' band Raman spectra, $I(\omega, E_{laser})$, is given as a function of the Raman shift, ω, and E_{laser} using the following formula:[4]

$$I(\omega, E_{laser})$$
$$= \sum_i \left| \sum_{a,b,\omega_1,\omega_2} \frac{M_{op}(i,c)M_{el\text{-}ph}(c,b)M_{el\text{-}ph}(b,a)M_{op}(a,i)}{\Delta E_{ai}(\Delta E_{bi} - \hbar\omega_1)(\Delta E_{ai} - \hbar\omega_1 - \hbar\omega_2)} \right|^2,$$

(1)

where $\Delta E_{ai} = E_{laser} - (E_a - E_i) - i\gamma$ is the energy denominator and γ denotes the Raman resonance width. i, a, b, and c denote the initial state, the excited state, the first scattered states, and the second scattered states of the photoexcited electron, respectively. For simplicity, only electron scattering

processes but no hole scattering processes were taken into account in this case. $M_{el\text{-}ph}$, and M_{op} show the electron-phonon and electron-photon interaction matrix elements, respectively, which were calculated using the ETB electronic wave function, and the force-constant tight-binding phonon modes. In the calculation of electron-phonon interaction matrix elements, the amplitude of the atomic vibration for each carbon atom was calculated for a large unit cell with a length of 1000 nm and at a temperature of 300 K. In the summation of the phonon frequencies ω_1 and ω_2, the energy-momentum conserved phonons, either for $M_{el\text{-}ph}(b,a)$ or for $M_{el\text{-}ph}(c,b)$, were selected to satisfy the double resonance condition, either for the incident resonance or for the scattered resonance, respectively.[4] For ω_1 and ω_2, $6 \times 2 \times 2 \times 2 = 48$ possible energy-momentum phonon modes can exist as far as the
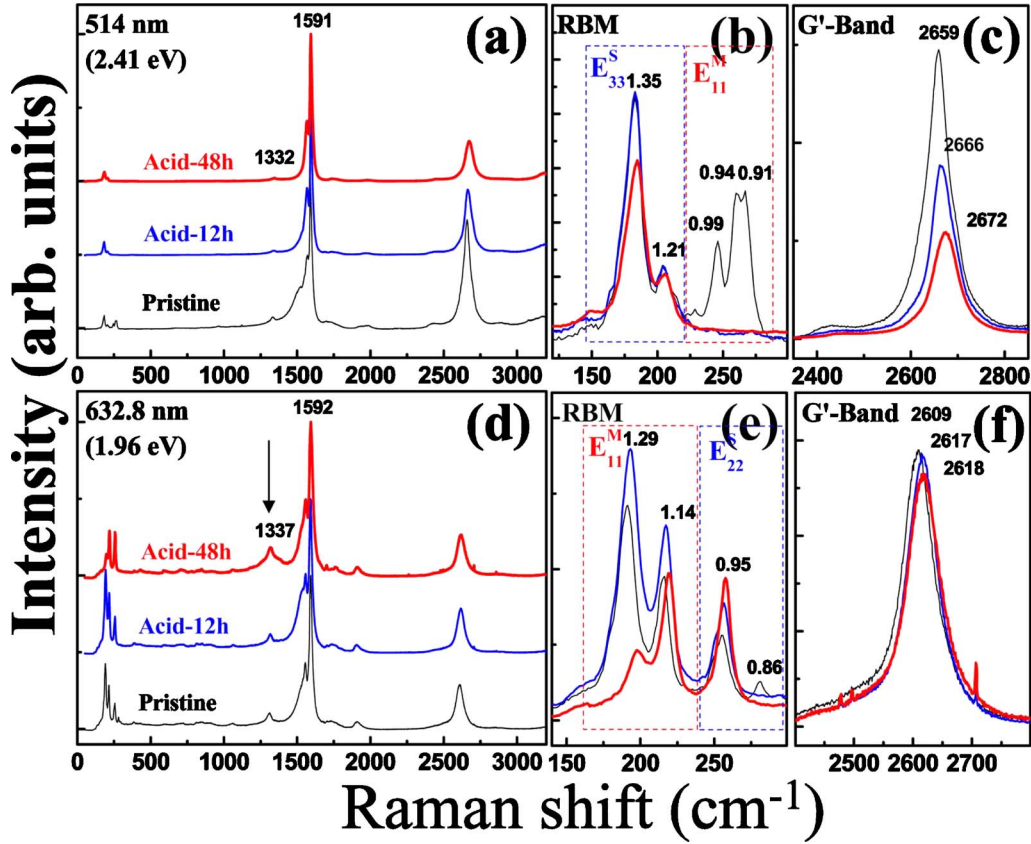
FIG. 3. (Color online) Raman spectra of the acid-treated HiPCO samples: pristine (bottom), for 12 h (middle), and for 48 h (top) at excitation energies of [(a)–(c)] 2.41 eV and [(d)–(f)] 1.58 eV. The notations are the same as shown in Fig. 1.

scattered electronic states are unoccupied because there are (1) six phonon modes in the two-dimensional (2D) graphite Brillouin zone, (2) two intraband and interband scatterings, where the intraband and interband scatterings denote the scattering of an electron from K to K (or K' to K'), and from K to K' (or K' to K', (3) two scattering directions (forward and backward scatterings), and (4) phonon absorption and emission. For the G' band intensity calculation, we select some of these possible cases, that is, two phonon modes [in-plane transverse optic (iTO) and in-plane longitudinal optic (iLO) mode], interband scattering, forward scattering, backward scattering, and only phonon emission. In the denominator of Eq. (1), the Raman resonance width γ in $\Delta E_{ai} = E_{laser} - (E_a - E_i) - i\gamma$ was calculated from the uncertainty principle for a finite lifetime of an electron due to the electron-phonon interaction for each (n,m) SWCNT using the Fermi golden rule.[25]

$$\gamma = \frac{\hbar}{\tau} = \hbar W_i = 2\pi \sum_f |\langle f|H_{el\text{-}ph}|i\rangle|^2 \delta(\varepsilon_f - \varepsilon_i). \quad (2)$$

Here, W_i represents the transition rate for the scattering of the photoexcited electron from an initial state i to all possible final states f by six phonon modes per unit time, satisfying the energy-momentum conservation. The calculated γ values were checked in order to reproduce the resonance width of

the Raman excitation profile for the RBM modes observed by single nanotube spectroscopy.[26]

III. RESULTS AND DISCUSSION

Figure 1 shows the Raman spectra of the pristine arc discharge SWCNTs with laser excitation energies at (a) 2.41 eV (514 nm), (b) 1.96 eV (632.8 nm), (c) 1.58 eV (785 nm), and (d) 1.165 eV (1064 nm). The corresponding RBM spectra were enlarged in the inset with phonon frequencies (bottom) and diameter (top). The numbers of G band and G' band show the phonon frequencies. All peak intensities were normalized to the G band intensity at 1589–93 cm^{-1}. For the 2.41 eV E_{laser}, the RBM spectra correspond to the E_{33}^S and E_{44}^S semiconductor resonance conditions that were assigned by the calculated Kataura plot by ETB model [Fig. 1(e)]. This assignment is consistent with the fact that the G band spectra do not show a metallic Breit-Wigner-Fano (BWF) line but a Lorentzian G band at the lower energy side [Fig. 1(a)].[27] The G' band was observed at 2680 cm^{-1}, in which the intensity of the SWCNT was not as strong as the G band intensity.

On the other hand, for the 1.96 eV E_{laser}, the RBM spectra could be assigned as being metallic (E_{11}^M) and semiconducting (E_{33}^S) SWCNTs, as shown in Fig. 1(b). This is despite the fact that a relatively strong RBM intensity in the semiconducting SWCNTs (163 cm^{-1}), strong BWF line in the G

TABLE I. Summary of the metallicity (M), D band intensity (D), and G' band intensity (G') normalized with respect to the G band intensity for all the samples in this work. The metallicity (%) was obtained by integrating each RBM of the Raman spectra by $100A_{\mathrm{metal}}/(A_{\mathrm{metal}}+A_{\mathrm{semi}})$, where A indicates the areal intensity of RBMs.

| | Excitation energy | | | | | | | | | | | |
| | 2.41 eV | | | 1.96 eV | | | 1.58 eV | | | 1.165 eV | | |
	M	D	G'	M	D	G'	M	D	G'	M	D	G'
Arc-Raw	0	0.006	0.17	24	0.026	1.03	100	0.07	0.29	0	0.09	0.08
NHFA-Raw	42.58	0.025	0.69	79.98	0.073	0.28	2.04	0.027	0.07			
NHFA-HTT	0	0.037	0.23	95.79	0.118	0.52	1.60	0.091	0.01			
Acid-Raw	40.35	0.027	0.71	83.58	0.063	0.28						
Acid-12h	0	0.013	0.42	86.25	0.053	0.28						
Acid-48h	0	0.011	0.26	64.49	0.118	0.26						

band, and prominent G' band intensity were also observed. This can be explained by the effect of a scattered photon resonance condition, in which the scattered resonance condition for the G' band appears at 0.32 eV lower than the incident resonance condition.[15] Therefore, for the 1.96 eV E_{laser}, the scattered resonance condition appears at approximately 1.64 eV, which corresponds to E_{11}^M for the frequency region (170–220 cm^{-1}) of the SWCNTs. On the other hand, the scattered photon (dashed line) condition for E_{11}^M also lies at E_{11}^M. Thus, the metallic SWCNTs in the sample enhance the BWF and G' band intensities, as shown in Fig. 1(b). For the 1.58 eV E_{laser}, only metallic SWCNTs were resonant in the RBM spectra, as shown in Fig. 1(c). Nevertheless, neither the BWF nor G' band intensity was as strong as those for 1.96 eV E_{laser}. This can be explained by the effect of the scattered photon, in which the scattered resonance condition for this E_{11}^M does not exist [perpendicular red line in Fig. 1(e)] for the given diameter region. This yields a relatively low G' band intensity compared with those observed with the 1.96 eV E_{laser}. For the 1.165 eV E_{laser}, the dominant contribution to the RBM spectrum is the semiconducting SWCNTs. Hence, the G' band had a weak intensity, as shown in Fig. 1(d). No scattered resonance condition from E_{22}^S was expected in this case.

The strong dependence of the G' band intensity on the metallicity of the SWCNTs was observed in the HiPCO samples, as shown in Fig. 2. The pristine HiPCO sample consists of both metallic and semiconducting SWCNTs for the 2.41 eV E_{laser}. After the NHFA treatment followed by thermal annealing at 900 °C, the metallic SWCNTs with small diameters were removed completely, while there were still semiconducting SWCNTs present without damage. This situation was confirmed by the significant reduction in BWF component in the G band shown in Fig. 2(a).[27] The G' band for the NHFA-treated sample was significantly suppressed because the metallic SWCNTs had been removed. If the metallic SWCNTs with a diameter of approximately 0.95 nm were present in the NHFA-treated sample, a strong G' band intensity would be expected due to the scattering resonance condition for the G' band at E_{11}^M. This suggests that the dependence of the G' band intensity on the metallicity is dominated by the incident photon resonance of the semiconducting SWCNTs. In the case of 1.96 eV E_{laser}, more metallic

tubes with large diameters remained in the sample, while the semiconducting SWCNTs with small diameters were suppressed after NHFA treatment. The BWF lines for the NHFA-treated sample were stronger than those for the pristine sample due to the higher metallic SWCNT component. In this case, the G' band intensity becomes stronger.

For 1.58 eV E_{laser}, the semiconducting SWCNTs can be resonant to E_{22}^S even after the NHFA treatment. The intensities of the G' band for both samples were much smaller than the G band intensity. However, the metallicity dependence of the G' band is not well recognized in this sample.

Figure 3 shows the result of the strongly acid-treated HiPCO sample. Nitronium ions that are generated in strong acid condition play a role in selectively attacking the metallic SWCNTs.[23,28] The degree of metallic SWCNT removal depends on the treatment time. For 2.41 eV E_{laser}, the amount of metallic SWCNTs and the G' band intensity decreased with increasing treatment time, which is consistent with the present metallicity dependence. For 1.96 eV E_{laser}, after a 12 h acid treatment, there was no significant difference in the RBMs and, subsequently, no difference in the G' band intensity. However, when the acid treatment was continued for up to 48 h, the metallic SWCNTs with large diameters were partially removed. Nevertheless, the G' band intensity did not change significantly from that of the pristine sample, while the D band intensity increased due to the formation of defects [see solid arrow in Fig. 3(d)].

Table I summarizes the D and G' band intensities relative to the G band intensity for various samples and excitation energies. The metallic SWCNTs clearly show a higher G' band intensity compared with the semiconducting SWCNTs. The amount of metallic SWCNTs was significantly reduced in the 48 h acid-treated sample. Nevertheless, the intensity of the G' band was not reduced further, but there was an increase in the D band. Although the D band and G' band are independent processes, both include the intervalley phonon scattering processes. More study will be needed to examine the relationship between the D band and G' band for defect-rich SWCNTs.

The G' band intensity was calculated for each E_{ii} value of (n,m) SWCNTs, whose intensity was normalized by per unit length of a SWCNT. Three variables were calculated to obtain the G' band intensity: the electron-phonon matrix ele-

iTO + iTO

iLO + iLO
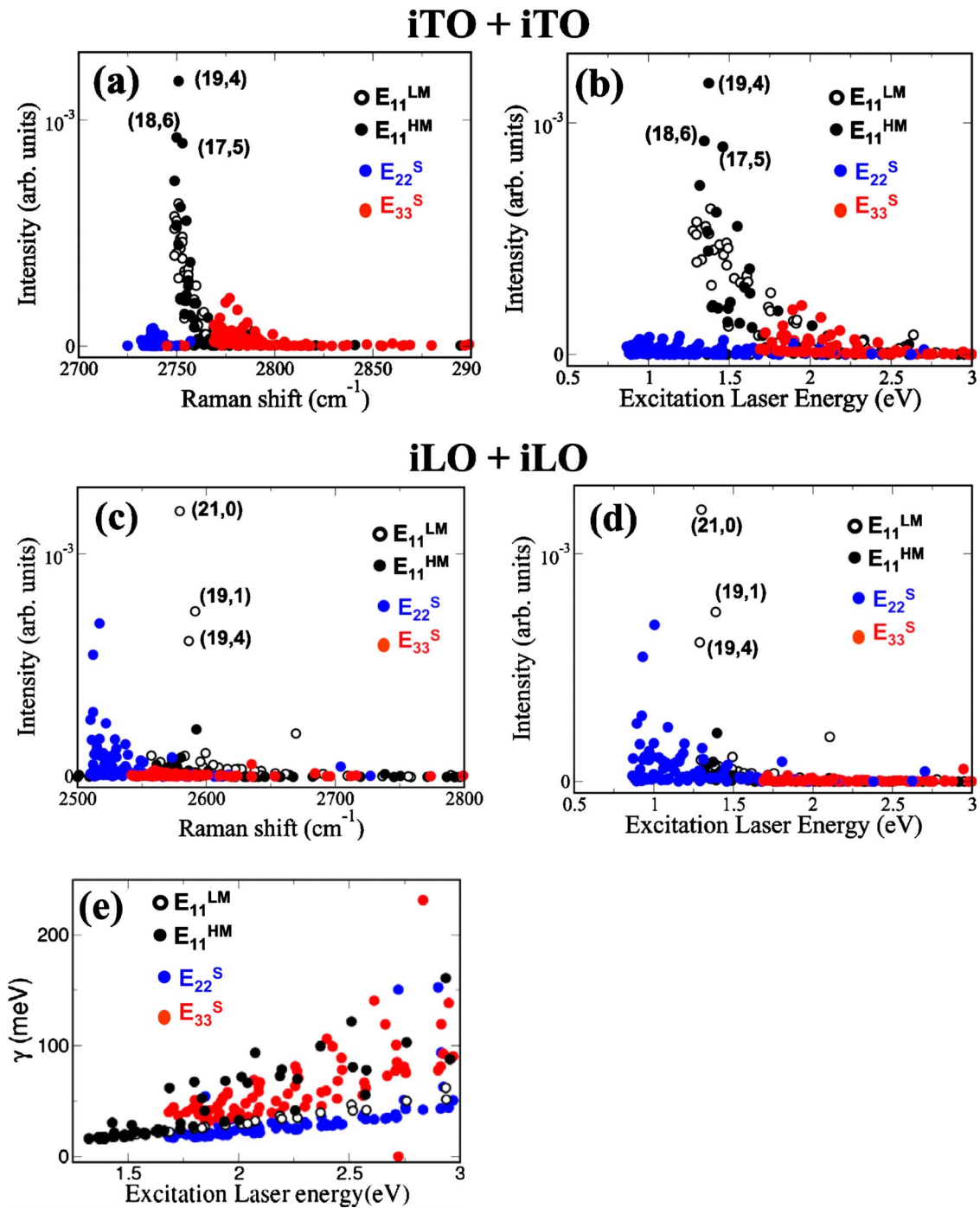
FIG. 4. (Color online) The calculated G' band Raman intensity as a function of (a) Raman shift and (b) laser excitation energy for iTO overtone. (c) and (d) are plotted as a function of the Raman shift and laser excitation energy for the iLO overtone, respectively. The blank and black filled circles indicate the lower E_{11}^M transition (E_{11}^{LM}) and the higher E_{11}^M transition (E_{11}^{HM}), respectively. (e) The resonance window, γ value, as function of the excitation laser energy. The blue and red filled circles indicate the E_{22}^S and E_{33}^S transitions, respectively.

ment, electron-photon matrix element, and γ value. Using the phonon dispersion relation of the SWCNT, the G' band might be related to a combination of the iLO and iTO phonon modes around the K point in the 2D graphite Brillouin zone.[4] Moreover, the electron-phonon matrix elements at the K point for the iTO phonon depend on the transition energy E_{ii}. The electron-phonon matrix element for the E_{11}^M transition for the metallic SWCNTs is larger than that for the E_{22}^S

transition of the semiconducting SWCNTs. The γ value was calculated using the relaxation rate from an excited state by emitting all types of phonons.[25]

Figure 4 shows the calculated G' band intensity by considering the iTO+iTO and iLO+iLO phonon combinations as a two-phonon process for all (n,m) SWCNTs in the diameter range $0.6 \leq d_t < 1.6$ nm. The iLO+iLO optical phonon combinations do not provide a metallicity dependence con-

sistent with the experiment for the G' band Raman intensity as shown in Figs. 4(c) and 4(d). It should be noted that the G' band by the iLO+iLO phonon combination provides a stronger intensity for semiconducting SWCNT than that for metallic SWCNT for $E_{laser} < 1.5$ eV. For excitation energies > 1.5 eV, a few metallic (n,m) tubes have a stronger intensity than semiconducting SWCNTs. However, electron-phonon matrix elements for the iLO phonon at the K point were independent of the metallicity.

For the combination of the iTO phonon, E_{11}^M provides a larger G' band intensity than E_{22}^S and E_{33}^S as shown in Figs. 4(a) and 4(b). When the reason for this behavior was examined, it was found that the electron-phonon matrix elements of the iTO phonon produce larger values for E_{11}^M than for E_{22}^S. For E_{33}^S, the electron-phonon matrix elements have a similar value compared to E_{11}^M. However, the γ value for E_{33}^S is larger than that for E_{11}^M, which reduces the Raman intensity for E_{33}^S as shown in Fig. 4(e). Because of the trigonal warping effect,[3] E_{11}^M, the vHs peak is split into two peaks at lower and higher energies, E_{11}^{LM} and E_{11}^{HM}, respectively. The G' band intensity for E_{11}^{LM} is definitely larger than that for E_{22}^S and E_{33}^S at all laser excitation energy ranges. The Raman shift for the G' band in the calculation was blueshifted (~ 100 cm^{-1}) compared with the experimental value. The agreement of the theoretical prediction with experiment values will be im-

proved if the Kohn anomaly,[29] which is more dispersive around the K point, is considered.

IV. SUMMARY

This study investigated a peculiar phenomenon in the G' band Raman intensity of SWCNTs. The intensity of the G' band was strongly related to the metallicity of the sample. This metallicity dependence was explained by electron-phonon interactions (mostly iTO phonon modes) from the extended tight-binding calculations. In addition, the effect of a scattered photon also contributed to the G' band intensity in some cases. These results demonstrate that the intensity of the G' band in Raman spectroscopy is a measure of the metallicity of carbon nanotube samples.

*Author to whom correspondence should be addressed.

†rsaito@flex.phys.tohoku.ac.jp

‡leeyoung@skku.edu

[1] R. Saito, M. Fujita, G. Dresselhaus, and M. S. Dresselhaus, Appl. Phys. Lett. **60**, 2204 (1992).

[2] K. H. An and Y. H. Lee, NANO **1**, 115 (2006).

[3] R. Saito, G. Dresselhaus, and M. S. Dresselhaus, Phys. Rev. B **61**, 2981 (2000).

[4] M. S. Dresselhaus, G. Dresselhaus, R. Saito, and A. Jorio, Phys. Rep. **409**, 27 (2005). For double resonance Raman spectroscopy, see R. Saito, A. Jorio, A. G. Souza Filho, G. Dresselhaus, M. S. Dresselhaus, and M. A. Pimenta, Phys. Rev. Lett. **88**, 027401 (2001).

[5] M. S. Strano, C. A. Dyke, M. L. Usrey, P. W. Barone, M. J. Allen, H. Shan, C. Kittrell, R. H. Hauge, J. M. Tour, and R. E. Smalley, Science **301**, 1519 (2003).

[6] J. Lefebvre, Y. Homma, and P. Finnie, Phys. Rev. Lett. **90**, 217401 (2003).

[7] M. J. O'Connell, S. M. Bachilo, C. B. Huffman, V. C. Moore, M. S. Strano, E. H. Haroz, K. L. Rialon, P. J. Boul, W. H. Noon, C. Kittrell, J. Ma, R. H. Hauge, R. B. Weisman, and R. E. Smalley, Science **297**, 593 (2002).

[8] A. M. Rao, E. Richter, S. Bandow, B. Chase, P. C. Eklund, K. A. Williams, S. Fang, K. R. Subbaswamy, M. Menon, A. Thess, R. E. Smalley, G. Dresselhaus, and M. S. Dresselhaus, Science **275**, 187 (1997).

[9] H. Kataura, Y. Kumazawa, Y. Maniwa, I. Umezu, S. Suzuki, Y. Ohtsuka, and Y. Achiba, Synth. Met. **103**, 2555 (1999).

[10] A. Jorio, R. Saito, J. H. Hafner, C. M. Lieber, M. Hunter, T. McClure, G. Dresselhaus, and M. S. Dresselhaus, Phys. Rev.

Lett. **86**, 1118 (2001).

[11] C. Journet, W. K. Maser, P. Bernier, A. Loiseau, M. L. Chapelle, S. Lefrant, P. Deniard, R. Lee, and J. E. Fischer, Nature (London) **388**, 756 (1997).

[12] L. C. Qin and S. Iijima, Chem. Phys. Lett. **269**, 65 (1997).

[13] W. Z. Li, S. S. Xie, L. X. Qian, B. H. Chang, B. S. Zou, W. Y. Zhou, R. A. Zhao, and G. Wang, Science **274**, 1701 (1996).

[14] M. Milnera, J. Kürti, M. Hulman, and H. Kuzmany, Phys. Rev. Lett. **84**, 1324 (2000).

[15] A. Jorio, A. G. Souza Filho, G. Dresselhaus, M. S. Dresselhaus, A. K. Swan, M. S. Ünlü, B. B. Goldberg, M. A. Pimenta, J. H. Hafner, C. M. Lieber, and R. Saito, Phys. Rev. B **65**, 155412 (2002).

[16] R. Saito, A. Jorio, J. H. Hafner, C. M. Lieber, M. Hunter, T. McClure, G. Dresselhaus, and M. S. Dresselhaus, Phys. Rev. B **64**, 085312 (2001).

[17] R. Saito, A. Jorio, A. G. Souza Filho, G. Dresselhaus, M. S. Dresselhaus, and M. A. Pimenta, Phys. Rev. Lett. **88**, 027401 (2001).

[18] J. Jiang, R. Saito, A. Grüneis, G. Dresselhaus, and M. S. Dresselhaus, Carbon **42**, 3169 (2004).

[19] J. Jiang, R. Saito, Ge. G. Samsonidze, S. G. Chou, A. Jorio, G. Dresselhaus, and M. S. Dresselhaus, Phys. Rev. B **72**, 235408 (2005).

[20] J. Jiang, R. Saito, K. Sato, J. S. Park, Ge. G. Samsonidze, A. Jorio, G. Dresselhaus, and M. S. Dresselhaus, Phys. Rev. B **75**, 035405 (2007).

[21] Y. S. Park, K. S. Kim, H. J. Jeong, W. S. Kim, J. M. Moon, K. H. An, D. J. Bae, Y. S. Lee, G. S. Park, and Y. H. Lee, Synth. Met. **126**, 245 (2002).

[22] K. H. An, J. S. Park, C. M. Yang, S. Y. Jeong, S. C. Lim, C. Kang, J. H. Son, M. S. Jeong, and Y. H. Lee, J. Am. Chem. Soc. **127**, 5196 (2005).

[23] C. M. Yang, J. S. Park, K. H. An, S. C. Lim, K. Y. Seo, B. S. Kim, K. A. Park, S. W. Han, C. Y. Park, and Y. H. Lee, J. Phys. Chem. B **109**, 19242 (2005).

[24] O. Dubay and G. Kresse, Phys. Rev. B **67**, 035401 (2003).

[25] J. S. Park, Y. Oyama, R. Saito, W. Izumida, J. Jiang, K. Sato, C. Fantini, A. Jorio, G. Dresselhaus, and M. S. Dresselhaus, Phys. Rev. B **74**, 165414 (2006).

[26] C. Fantini, A. Jorio, M. Souza, M. S. Strano, M. S. Dresselhaus, and M. A. Pimenta, Phys. Rev. Lett. **93**, 147406 (2004).

[27] S. D. M. Brown, A. Jorio, P. Corio, M. S. Dresselhaus, G. Dresselhaus, R. Saito, and K. Kneipp, Phys. Rev. B **63**, 155414 (2001).

[28] K. Y. Seo, K. A. Park, C. W. Kim, S. W. Han, B. S. Kim, and Y. H. Lee, J. Am. Chem. Soc. **127**, 15724 (2005).

[29] J. Maultzsch, S. Reich, C. Thomsen, H. Requardt, and P. Ordejon, Phys. Rev. Lett. **92**, 075501 (2004).